Polymer 49 (2008) 4673–4679

Contents lists available at ScienceDirect

Polymer

journal homepage: www.elsevier.com/locate/polymer

Surface structure of folded-chain crystals of poly(*R*-3-hydroxybutyrate) of different chain length

René Androsch*

Martin-Luther-University Halle-Wittenberg, Center of Engineering Sciences, D-06099 Halle/Saale, Germany

ARTICLE INFO

Article history:
Received 25 June 2008
Received in revised form 11 August 2008
Accepted 13 August 2008
Available online 19 August 2008

Keywords:
Poly(*R*-3-hydroxybutyrate)
Rigid amorphous fraction
Reversible crystallization and melting

ABSTRACT

The structure of the crystalline–amorphous interface of poly(*R*-3-hydroxybutyrate) (PHB) of different molar mass is evaluated by analysis of the rigid amorphous fraction and by analysis of the degree of reversible melting and crystallization. The rigid amorphous fraction of low-molar-mass PHB of 5 kDa is only 5–10%, and at best half of that of high-molar-mass PHB of almost 500 kDa, despite identical crystallinity. This result is paralleled by observation of distinctly larger degree of reversible melting and crystallization in PHB of high molar mass. The larger rigid amorphous fraction and higher degree of reversible melting and crystallization in PHB of high molar mass, consistently and independently, prove enhanced covalent coupling of crystals and amorphous structure, and/or de-coupling of segments of macromolecules which traverse between phases, respectively. The distinct isolation of crystals in PHB of low molar mass is discussed in terms of absence of wide loops/folds, long-chain cilia, and tie-molecules.

1. Introduction

The crystalline and amorphous phases in semi-crystalline polymers coexist within a meta-stable arrested thermodynamic equilibrium, and would only be linked by physical bonds at the top and bottom crystal surfaces if phase-traversing molecule segments do not exist. The link between crystals and amorphous phase, partially, is of covalent nature if molecule segments cross the phase boundary. In folded-chain crystals, in general, the number of molecules which cross the crystalline–amorphous interface is reduced by frequent adjacent re-entry of chains at the crystal top and bottom surfaces, forming folds. In fringed micelles, in contrast, the number of phase-traversing molecules per unit area is increased, which is indicated by a (5–10)× higher specific surface free-energy than in case of a fold surface [1–3]. The coupling of phases, i.e., the surface structure of crystals, affects properties of both crystalline and amorphous phases, including the temperature of melting of crystals [3–5], the glass transition temperature [6–8], or the free volume of the amorphous phase [9] and controls, therefore, the overall materials behavior [10]. Quantification of the covalent coupling of crystalline and amorphous phases, at present, is by far not achieved, however, essential for full characterization of the structure and control of the properties of semi-crystalline polymers. The present study is an attempt to further develop this field of research by analysis of the link between the crystalline and amorphous phases in PHB of different molar mass.

Quantification of the linkage between crystalline and amorphous phases is possible by analyses of the rigid amorphous fraction and of the degree of reversible crystallization and melting. Molecule segments in the amorphous phase exhibit a reduced mobility if they are covalently connected with the crystalline phase. This part of the amorphous phase, commonly, is named rigid amorphous fraction (RAF), and was identified in numerous semi-crystalline polymers since it first discovery about 25 years ago [11–13]. We assume that the restriction of parts of the amorphous phase depends on the number of chain segments which cross the crystal–amorphous interface. However, this is not yet unequivocally proven by experiment, since a variation of the crystal-surface structure, i.e., of the number of phase-crossing chains, independent of crystallinity, crystal size and crystal-defect concentration, seems impossible. First attempts for establishing a relationship between the crystal morphology and RAF at least demonstrated that the RAF indeed is controlled by the specific crystal-surface area and the perfection of crystals [14–16].

A different option to access information about the crystalline–amorphous interface in semi-crystalline polymers is the analysis of the degree of reversible melting and crystallization [17,18]. Reversible melting and crystallization in semi-crystalline polymers is denoted to melting and crystallization, which does not need nucleation, and which occurs therefore path-independent in equilibrium with temperature. Reversible melting and crystallization only is possible at the surface of crystals, employing selected molecule segments which are kept in a state of lowered entropy when melted. Reversible melting and crystallization has been identified to occur at fold-surfaces of crystals of polymers which are

* Tel.: +49 3461 46 3762; fax: +49 3461 46 3891.
E-mail address: rene.androsch@iw.uni-halle.de

0032-3861/$ – see front matter © 2008 Elsevier Ltd. All rights reserved.
doi:10.1016/j.polymer.2008.08.026

able for chain-sliding diffusion [19–21] and, as a general phenomenon, at the lateral growth-faces [22–24]. The degree of reversible melting and crystallization, which is the amount of phase-converted matter per temperature change [25], has been shown to be significantly affected by the crystal morphology [26–28]. This conclusion was derived by systematic investigation of reversible melting and crystallization of extended-chain crystals, folded-chain crystals and fringed micelles, which, in that order, get increasingly coupled to the surrounding amorphous phase. As a result of the increasing covalent linkage between phases, the degree of reversible melting was increased. In the present study, we intend to test whether reversible melting can be used as a probe for analysis of the fine-structure of the crystalline–amorphous interface of PHB of different molar mass, and whether reversible melting is related to the RAF.

We selected for the present study PHB since it shows reversible melting and forms a RAF [13,29–34]. For example, calorimetric analysis of structure formation during isothermal cold-crystallization at 296 K led to the conclusion that the RAF forms and vitrifies during crystallization. After completion of the crystallization process, the sample consisted of 64% crystalline phase, 24% RAF, and 12% mobile amorphous fraction (MAF) [29,30]. In the same study, PHB was quenched below the glass transition temperature, which yielded an initially completely amorphous sample. Subsequent, slow heating triggered cold-crystallization at about 300 K, and melting at temperatures close to 450 K. Within the temperature range of final melting, considerable excess-apparent-heat capacity was detected, which indicated reversible melting. Correlations between RAF, degree of reversible melting, and the crystal morphology were not established.

In order to identify such a relation in the present work, we employed two, molecularly well-defined PHB of different molar mass of 5 and 437 kDa (PHB-5000 and PHB). Both preparations are semi-crystalline, and form on melt-crystallization folded-chain lamellae, which are arranged within spherulites [35–37]. With the analysis of the RAF and of the degree of reversible melting, we intend to prove different coupling of folded-chain crystals and amorphous structure in these specimen. Reduced coupling is expected in PHB-5000, since recent X-ray analyses of the crystal thickness led to the conclusion that the length of loose ends or cilia, respectively, probably is reduced to the non-crystallizing end-groups.

In the first part of this work, we describe the crystallization of PHB-5000 from the glassy state, which allows generation of samples of different crystallinity. In the second part, crystallization from the liquid state of both PHB-5000 and PHB is explained. The analysis of the RAF and of reversible melting is presented in next chapter, followed by a discussion in terms of the crystal morphology and the crystalline–amorphous interface.

2. Experimental

2.1. Materials

Natural PHB with a mass-average molar mass of 437 kDa and a polydispersity of 1.67 was obtained by Sigma Aldrich (Cat number 36,350-2, Lot number S17920-224). The PHB of molar mass of 5 kDa (PHB-5000) was purchased from Polysciences (Cat number 16938, Lot number 557223), and is terminated by an allylic group and a carboxylic group.

2.2. Instrumentation

2.2.1. Standard differential scanning calorimetry (DSC)

We used a power-compensation-type DSC 7 from Perkin–Elmer, which was equipped with the cryogenic cooling accessory CCA 7, using liquid nitrogen as coolant. Furnaces were purged with gaseous nitrogen at a flow rate of 35 mL min^{-1}. The heat sink temperature was 213 K, which was selected to ensure accurate analysis of the glass transition at about 270–280 K. The instrument was calibrated with respect to temperature and heat-flow rate, using standard procedures, as are described in text books [38,39]. Heat-flow-rate raw data were converted into apparent specific heat capacities after subtraction of an instrumental baseline, measured under identical conditions as the sample, and ensuring identical mass of pans in the baseline- and sample-runs. Apparent-heat-capacity data finally were corrected using sapphire as standard. We used 20 μL aluminum pans from Mettler-Toledo for encapsulation of the samples. The sample mass, typically, was 2–5 mg, and the rate of heating was 20 K min^{-1}, if not stated otherwise. Standard DSC was employed for analysis of the RAF, and the determination of the enthalpy-based crystallinity of samples. Details about the calculation of the RAF and of the crystallinity as a function of temperature are described elsewhere [8,40,41]. For the crystallinity-calculation, a bulk heat of fusion of the PHB crystal of 146 J g^{-1} was used [35].

2.2.2. Temperature-modulated differential scanning calorimetry (TMDSC)

The determination of the degree of reversible melting and crystallization is based on the measurement of the heat capacity in the absence of irreversible processes. This requires prior equilibration of structure, which can only be achieved by isothermal experimentation [42]. Any variation of temperature in semi-crystalline polymers triggers renewal of irreversible equilibration, and, consequently, reversible and irreversible processes overlap. The heat capacity was measured using quasi-isothermal temperature modulation with an amplitude of 1 K, i.e., an amplitude which is sufficiently small to allow equilibration of structure. The modulation period was 120 s. Similar as in standard DSC, modulated heat-flow-rate raw data were corrected for instrumental asymmetry before conversion into apparent heat capacities, and finally corrected by sapphire. Details regarding the data reduction by discrete Fourier transformation are described elsewhere [43]. Reversible melting and crystallization is recognized by detection of excess heat capacity. Excess heat capacity is defined as difference between the measured, apparent heat capacity, after structural equilibrium has been achieved, and the expected, vibration-based heat capacity of the semi-crystalline sample.

2.2.3. Atomic force microscopy (AFM)

For PHB of high molar mass, formation of lamellae and of higher-order, spherulitic structure is well-documented in the literature [35,36,44]. The spherulitic superstructure of melt-crystallized PHB-5000, we investigated recently [37]. Microscopic data about the crystal morphology of low molar mass analogues of PHB were gained on solution-crystallized preparations [36,45], however, are not available yet for the specific, melt-crystallized PHB-5000 of the present work. Therefore, we employed AFM for validation of formation of lamellae in PHB-5000 in the present study. Specimens were crystallized in presence of mica, which served as a substrate for generation of a smooth surface, using an identical temperature–time profile as in DSC-crystallization experiments. The AFM was a Quesant Q-Scope 250 with a 40 μm × 40 μm scanner. We used standard silicon cantilevers NSC 16, with a force constant of 40 N m^{-1} and resonant frequency of about 170 kHz. Images were collected in non-contact mode.

3. Results and initial discussion

3.1. Crystallization of PHB-5000 from the glassy state

Fig. 1a shows the apparent specific heat capacity of PHB-5000 of different crystallinity as a function of temperature in the

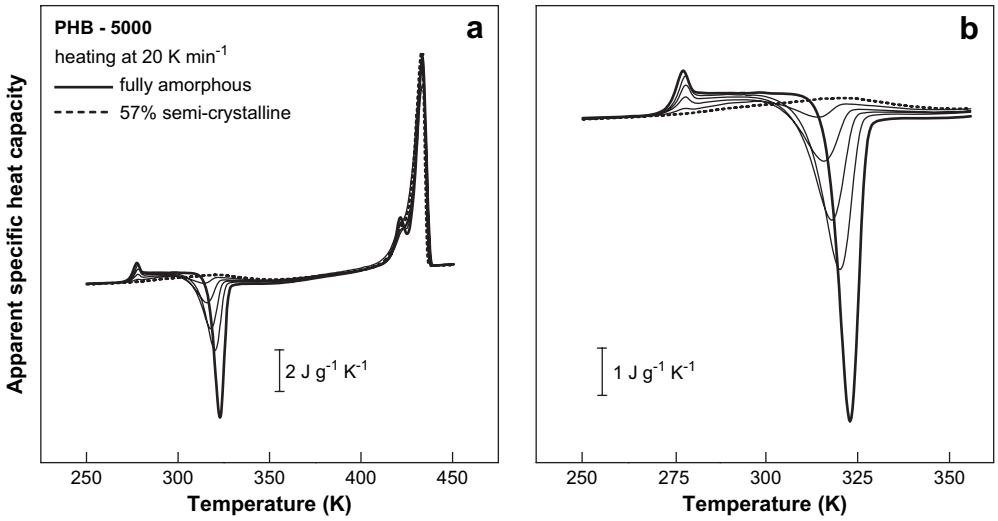

Fig. 1. Apparent specific heat capacity of PHB-5000 of different initial crystallinity as a function of temperature, obtained on heating at a rate of 20 K min^{-1}: (a) overview; (b) enlargement of (a), showing details of the glass transition and of cold-crystallization.

temperature-range between 250 and 450 K, observed on heating at a rate of 20 K min^{-1}. Fig. 1b is an enlargement, showing details of the glass transition and subsequent cold-crystallization. Samples of different initial crystallinity were prepared by quenching liquid samples from 473 to 290 K, and cold-crystallization for different periods of time at 300 K. Isothermal cold-crystallization was completed after about 60 min, and led to a semi-crystalline sample with a degree of crystallinity of close to 60%. Interruption of the cold-crystallization, before it was completed, by cooling to 238 K, i.e., to a temperature lower than the glass transition temperature, allowed preparation of samples of variable crystallinity for subsequent analysis of the RAF. The thick solid line in Fig. 1 represents data, which were obtained on a fully amorphous sample. The glass transition is observed at about 274 K, and is superimposed by an endothermic enthalpy relaxation. The heat capacity increases on devitrification by about 0.5 J g^{-1} K^{-1}, which is the expected increment for a fully amorphous sample [29]. Further heating triggers cold-crystallization, which starts at about 300 K, and melting which is completed at about 440 K. The thin solid lines are data which were collected on semi-crystalline samples with a crystallinity between 12 and 52%. Increasing the initial crystallinity is connected with a decrease of the heat-capacity increment at the glass transition, and a decrease of the heat-of-cold crystallization. The temperature and heat of final melting do not seem to be affected by the history of crystallization. The dotted line was obtained on a sample of almost 60% crystallinity. This preparation, at best, shows a glass transition which is extremely broadened towards high temperature. A step-like increase of the heat capacity within a narrow temperature-range, as in specimens of lower crystallinity, is not detected using standard DSC. Absence of cold-crystallization in the vicinity of 300 K indicates that the initial, isothermal cold-crystallization at 300 K was completed.

Initially quenched and subsequently at 300 K isothermally cold-crystallized PHB-5000 yielded a maximum enthalpy-based crystallinity of 57%. The crystallinity was further increased to 75% by annealing at 403 K. Fig. 2 shows with the solid curve the apparent specific heat capacity of fully amorphous PHB-5000, obtained by standard DSC, using a heating rate of 20 K min^{-1}. Absence of crystals in this specimen is indicated by matching the heat capacities of fully solid and liquid PHB [29], before and after devitrification. This curve ends at 300 K, because the sample was then isothermally cold-crystallized for a period of 60 min. Subsequently, the sample was cooled to 238 K, before analysis of the glass transition by standard DSC and by TMDSC. In Fig. 2, as an example, TMDSC data are shown with the open squares. The advantage of using TMDSC, in comparison with standard DSC, is a reduced error in determination of the heat-capacity increment at the glass transition since data after sufficiently long quasi-isothermal modulation are not affected by superimposed irreversible processes. TMDSC data were recorded up to a maximum temperature of 323 K. The cold-crystallized sample was then further heated to 403 K, isothermally annealed for a period of 60 min, and cooled again to 238 K. The subsequent analysis of the glass transition of such a cold-crystallized and at elevated temperature additionally annealed sample is shown with the filled squares. The increase of the enthalpy-based crystallinity from 57 to 75%, due to annealing at 403 K, leads to a further reduction of the heat capacity increment on devitrification.

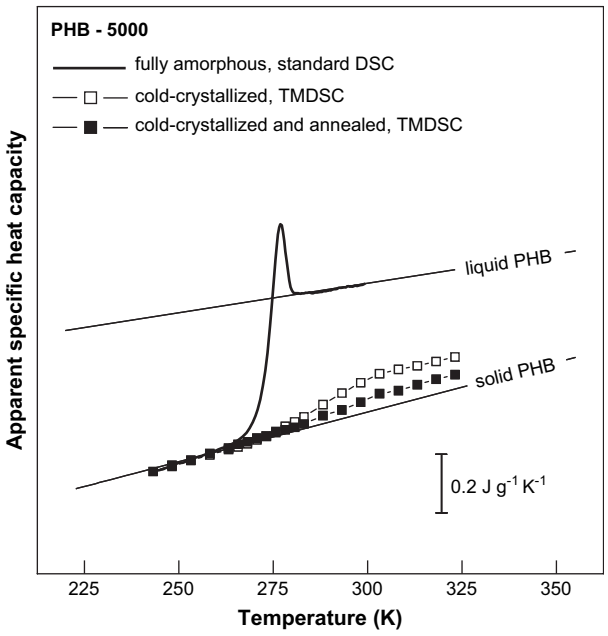

Fig. 2. Apparent specific heat capacity of PHB-5000 as a function of temperature in the temperature-range of the glass transition. The thick solid curve was obtained on fully amorphous PHB-5000 by standard DSC, and the symbols represent heat-capacity data of cold-crystallized (open squares), and cold-crystallized and at 403 K annealed PHB-5000 (filled squares), obtained by TMDSC. The thin lines are heat capacities of fully solid and liquid PHB.

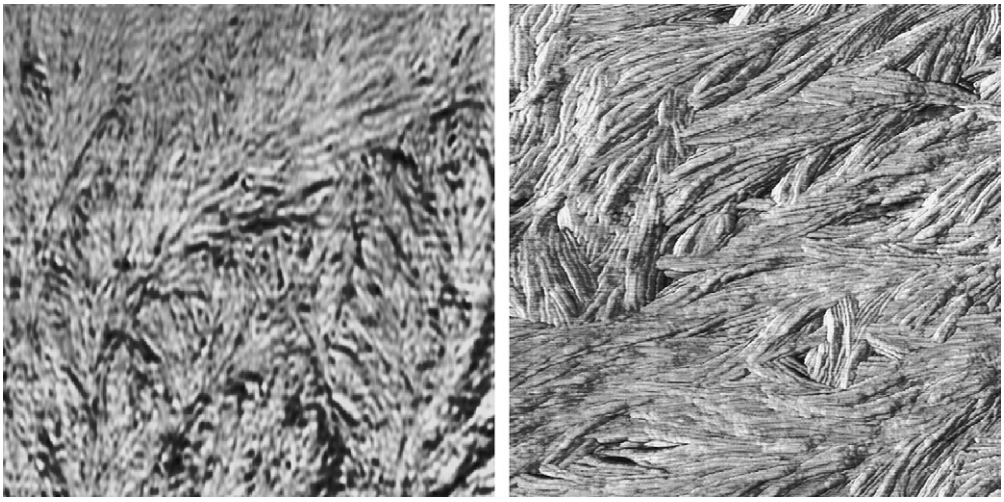

Fig. 3. AFM phase-images of cold-crystallized PHB-5000 (left), and cold-crystallized and at 403 K annealed PHB-5000 (right). The image size is 1 μm × 1 μm.

The crystal morphology of PHB-5000, which initially was crystallized from the glassy state, is analyzed using AFM. The left image in Fig. 3 was obtained on a sample which was isothermally cold-crystallized at 300 K, and the right image was obtained after additional annealing at 403 K. The images were taken at ambient temperature, and the scan size is 1 μm × 1 μm. Cold-crystallization results in formation of rather short, and frequently branched lamellae of extremely low thickness of about 5 nm. Subsequent annealing at elevated temperature allows thickening of lamellae. Manual estimation of the thickness suggests values of about 10 nm. The images furthermore reveal a considerable increase of the crystallinity as result of annealing.

3.2. Crystallization of PHB-5000 and PHB from the liquid state

Crystallization of PHB-5000 from the liquid state was performed in order to produce crystals of different morphology and thermodynamic stability, respectively, in comparison to the crystallization from the glassy state. Crystallization from the glassy state, at high super-cooling, usually, generates rather small crystals due to the high number of nuclei, and low critical size of nuclei. Crystallization from the liquid melt occurs at lower super-cooling, and crystals are therefore expected to be larger, and perhaps differently coupled to the surrounding amorphous phase. Samples were crystallized under non-isothermal conditions at rates of cooling between 1 and 50 K min^{-1}. The maximum temperature of the melt was 448 K, which needs to be reported, since it affects the kinetics of crystallization. Fig. 4a shows the apparent specific heat capacity of melt-crystallized PHB-5000 in the temperature-range of the glass transition. Non-isothermal melt-crystallization at 20 and 50 K min^{-1} yielded samples with enthalpy-based crystallinities of 70 and 63%, respectively. From these crystallinity-data, the expected heat capacity after complete devitrification has been calculated, which is indicated with the dashed lines of a thickness which is related to the measured curves. Visual inspection of measured and expected heat capacities indicates that the devitrification of the amorphous phase is incomplete at the glass transition of the MAF, i.e., at a temperature close to 280 K.

Fig. 4b is a similar experiment on PHB of high molar mass. PHB was heated to 458 K, equilibrated for a period of 3 min, and subsequently melt-crystallized at different rate of cooling. In Fig. 4b is shown the subsequent analysis of the apparent specific heat capacity in the temperature-range of the glass transition, by heating at 20 K min^{-1}. In this example are presented data, which were obtained on samples cooled at 10 and 40 K min^{-1}. The crystallinity of these preparations is 61 and 51%, respectively. The expected heat capacity after complete devitrification of the amorphous phase is shown with the dashed lines, as in Fig. 4a. The mismatch between the measured and expected data proves the existence of a non-devitrified part of amorphous structure, i.e., of a RAF.

3.3. Rigid amorphous fraction and reversible melting

The heat capacity increment at the glass transition of the mobile amorphous phase of samples of largely different crystallinity has been used for calculation of the RAF. Fig. 5 is a plot of the RAF at the glass transition of the MAF, as a function of the enthalpy-based crystallinity. The graph includes data of both PHB-5000, and PBH, as are denoted in the legend. The diagonal line represents the total

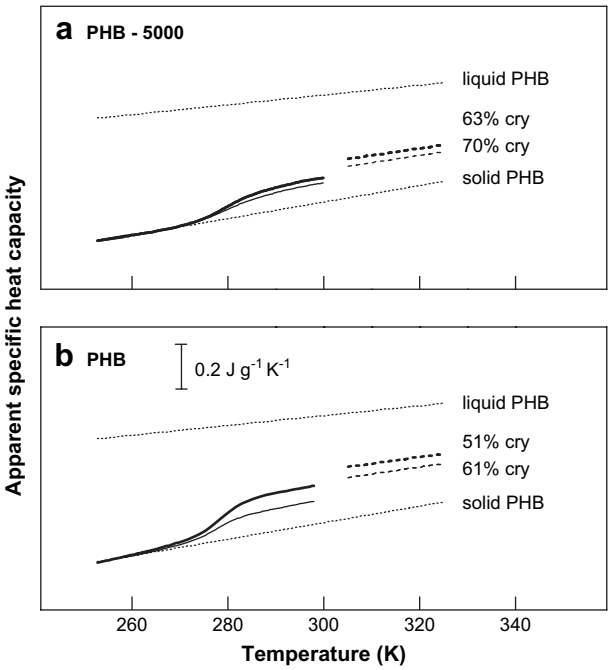

Fig. 4. Apparent specific heat capacity of (a) PHB-5000 and (b) PHB as a function temperature in the temperature-range of the glass transition. Samples were melt-crystallized at different rates of cooling, as described in the text. The graphs include heat capacities of fully liquid and solid PBH (dotted lines). Expected heat capacities of completely devitrified, semi-crystalline samples are indicated for the samples of different crystallinity by the dashed lines.

amorphous fraction. The difference between this line and the RAF data identifies the MAF. The RAF of PHB-5000 is almost independent on the crystallinity, and is at best about 5–10% of the total structure. The RAF of PBH of high molar mass is about 20% of the total structure, i.e., it is about twice the RAF of PHB-5000. As a guide for the eye, we have included in Fig. 5 horizontal lines, which allow an easier comparison of the RAF in PHB-5000 and PHB. The RAF data, which we obtained on PHB (open squares) agree well with data of an independent study (filled square), which revealed 24% RAF for cold-crystallized PHB of 64% crystallinity [29]. Despite we observed different RAF in PHB-5000 and PHB, the total amount must be considered as rather low. Fig. 5 contains, for comparison, RAF data of poly(ethylene terephthalate) (PET), which were collected in a recent study [16]. The RAF in PET is considerably larger than in PHB of similar, low crystallinity. The low absolute amount of RAF in PHB and PHB-5000 results in a relatively large error of measurement. In particular the data observed on samples of PHB-5000 which were crystallized from the glassy state reveal the typical error of heat capacity measurements with the used instrumental setup. The maximum heat-capacity increment at the glass transition of the MAF is $0.5\,J\,g^{-1}\,K^{-1}$. Allowance of an instrumental inaccuracy of $\pm 0.02\,J\,g^{-1}\,K^{-1}$ yields a minimum error of the RAF of ±4%. For this reason, we consider the RAF data of the present work at best as semi-quantitative.

Fig. 6 shows the apparent specific heat capacity of PHB-5000 (filled squares) and PHB (open symbols, stars) as a function of temperature, in the temperature-range of final melting. Data were collected by quasi-isothermal TMDSC, after structural equilibrium has been achieved. PHB-5000 was non-isothermally melt-crystallized at a rate of cooling of $1\,K\,min^{-1}$, and subsequently heated stepwise at the same rate, in between the quasi-isothermal temperature-modulation segments. The crystallinity of 73% of this sample, after completed crystallization, was estimated by standard DSC, using identical rates of temperature change, and omitting the quasi-isothermal segments. Similarly, PHB was non-isothermally melt-crystallized, using different rates of cooling between 10 and $40\,K\,min^{-1}$. Despite the rate of cooling slightly affected the

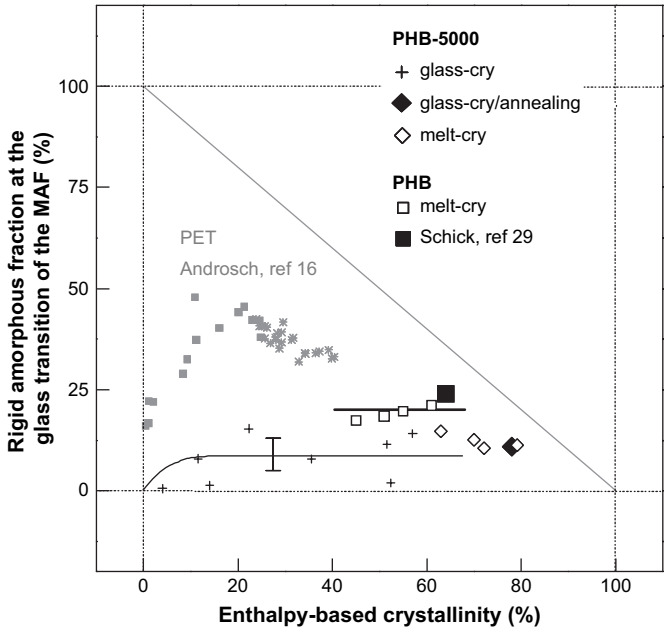

Fig. 5. Rigid amorphous fraction at the temperature of the glass transition of the MAF of PHB-5000 and PHB of different history of crystallization as a function of enthalpy-based crystallinity. The diagonal line indicates the total amorphous fraction. The gray symbols show RAF data which were obtained on poly(ethylene terephthalate) in a recent study [16], and were included for comparison.

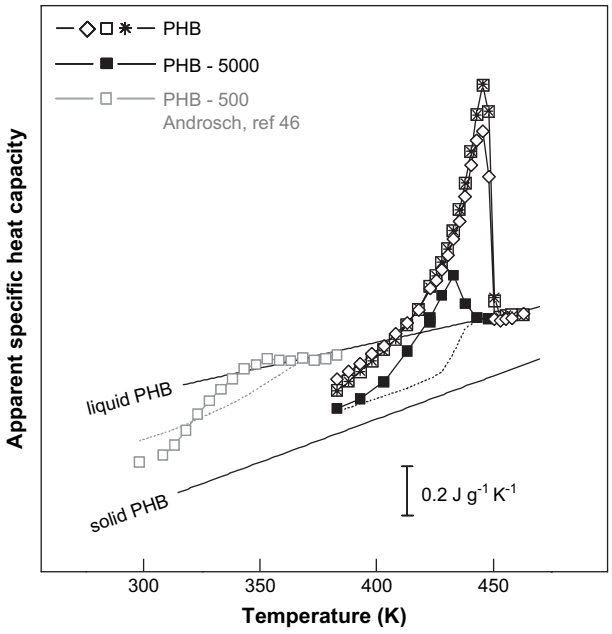

Fig. 6. Apparent specific heat capacity of PHB-500 (gray open squares) [46], PHB-5000 (filled squares) and PHB (open symbols, stars) as a function of temperature. Data were collected using quasi-isothermal TMDSC, after completion of irreversible equilibration of structure. The plot includes with the solid lines heat capacities of liquid and solid PHB, and with the gray and black dotted lines the vibration-based heat capacity of semi-crystalline PHB-500 and PHB-5000, respectively.

crystallinity, the equilibrium-apparent-specific-heat capacity on subsequent melting is indifferent of this parameter. The data of Fig. 6 reveal occurrence of reversible melting and crystallization, which is concluded from the detected excess heat capacity, i.e., heat capacity of the meta-stable, equilibrated samples in excess of the vibrational heat capacity. For PHB-5000, the vibrational heat capacity is shown with the dotted line. Accordingly, the maximum excess heat capacity of this sample is about $0.3\,J\,g^{-1}\,K^{-1}$. For PHB, most striking, the estimated maximum excess heat capacity is about $1\,J\,g^{-1}\,K^{-1}$, i.e., it is more than 3× larger than in PHB-5000. Further support for observation of a distinct effect of the length of molecules on the maximum excess heat capacity is provided with recently collected data [46], which were obtained on a specific semi-crystalline sample of molar mass of $500\,g\,mol^{-1}$ (gray squares). In this case the maximum excess heat capacity is even lower than in case of PHB-5000.

4. Final discussion and conclusions

Recent research of the crystallization and melting behavior and of the structure of PHB provided evidence for reversible crystallization and melting, and for formation of a rigid amorphous fraction in semi-crystalline preparations [13,29–34]. Reversible crystallization and melting and formation of a RAF both must be considered as measures of the covalent linkage between the crystals and surrounding amorphous structure. In the present study, we extend the research on PHB, and attempt to explore the effect of the chain length on the covalent linkage between the crystalline and amorphous phases. The experimental data of Figs. 5 and 6 show that PHB of high molar mass exhibits a considerably larger RAF and degree of reversible melting, despite similar crystallinity and crystal shape as in case of PHB-5000. The PHB of molar mass of 5 and 500 kDa, which can be employed for a comparison, exhibit an approximate crystallinity of 60–70%, and show formation of lamellae as dominant crystal form, organizing in a spherulitic superstructure. These information justify the assumption of similar total area of the

bottom and top surfaces of crystals in both PHB of largely different molar mass. The observation of different RAF and degree of reversible crystallization and melting must then be attributed to different structure of the top and bottom crystal surfaces.

The contour length of molecules in PHB-5000 and PHB is about 17–20 and 1700 nm, respectively, assuming a conformation of the molecules as in the crystalline state [35,47]. The crystal thickness in both PHB-5000 and PHB, typically is 5–10 nm [35,37]. These information allow to conclude that the occurrence of tie-molecules, and of long-chain cilia in PHB-5000 is negligible. Even if the molecule contributes to only two stems, i.e., if it forms only a single fold, then the remaining average length of the molecule, which enters the amorphous phase is much less than 5 nm. In PHB of high molar mass, in contrast, formation of tie-molecules, long-chain cilia, and wide loops is not restricted a priory by the length of the molecules. On the other hand, a decrease of the molar mass to 500 g mol^{-1} results in formation of extended-chain crystals [37]. Covalent coupling between crystals and amorphous phase is then minimized and even less evident than in PHB-5000, as is indicated by the reduced degree of reversible melting and crystallization (Fig. 6) [46].

Fig. 7 is an illustration of the structure of lamellae and its linkage to the amorphous phase in PHB-5000 (left) and in PHB (right). The circles in the sketch of the structure of PHB-5000 represent the two different end-groups of the molecule. The thickness of the crystalline and amorphous layers is selected to achieve a linear crystallinity of 60%, and the gray-shaded layers at the bottom and top surfaces of crystals visualize the RAF, approximating the results of Fig. 5. In PHB-5000, the immobilization of the amorphous phase due to presence of crystals is negligible, i.e., the ratio between RAF and MAF is less than unity. In PHB of high molar mass, the crystalline and amorphous phases are coupled to distinctly higher degree due to a larger number of molecules which simultaneously are part of both phases, indicated with the bold-drawn molecules in Fig. 7.

The RAF data of Fig. 5 provide information about the phase composition in PHB-5000 and PHB. The exact nature of the crystalline–amorphous interface, however, cannot be directly derived from these data. In other words, further analytical evidence is required to support our view of the fine-structure of the crystal surfaces, as is suggested with the illustrations in Fig. 7. In the present study we employed an analysis of the degree of reversible crystallization and melting for characterization of the structure of the crystal basal planes. Reversible crystallization in polymers is suggested to occur by crystal growth in chain direction [19–21], or in lateral direction [22–24]. Reversible crystal growth in chain direction, we do not consider as the major mechanism in the present case since it requires mobility of amorphous molecule segments near the crystal basal planes, in combination with capability of the polymer to perform chain-sliding diffusion through the crystal. Reversible crystallization and melting at the lateral surfaces of crystals by attachment/detachment of complete stems, in contrast, is not restricted by presence of a RAF at the crystal basal planes, and the capability for intra-crystalline chain-diffusion. The only requirement for nucleation-free, reversible crystallization and melting of molecule segments at existing lateral crystal faces is the preservation of a state of lowered entropy after melting, in order to avoid repeated molecular nucleation before it can re-crystallize [4]. Preservation of a state of a lower entropy of the particular molecule segment, which crystallizes and melts reversibly, for instance, may be achieved if the molecule does not melt completely, i.e., if there remains a molecular nucleus. This can be achieved by covalent linkage of the reversibly crystallizing/melting molecule segment to different crystals, if it is a tie-molecule, or to other parts of the same crystal, if there is evident a wide loop at the fold surface. The data of Fig. 6 explicitly support this view of the process of reversible crystallization and melting. The maximum reversible change of crystallinity per Kelvin temperature change is 0.7% K^{-1} ($= 1\ J\ g^{-1}\ K^{-1}/146\ J\ g^{-1} \times 100\%$) in PHB of high molar mass, and only 0.2% K^{-1} ($= 0.3\ J\ g^{-1}\ K^{-1}/146\ J\ g^{-1} \times 100\%$) in PHB-5000. Fig. 8 summarizes the main structural details of the crystal surfaces in PHB-5000 (left) and PHB (right). It shows with the top sketches a crystal before initiation of melting by a small increase of temperature, as was realized in the TMDSC experiment. At the lateral crystal face, an unstable patch of three stems is assumed to melt on heating, as is indicated with the bottom sketches. In PHB-5000, melting of a three-stem patch involves melting of the complete molecule, which immediately adopts the entropy of the liquid. Subsequent cooling does not allow crystallization/attachment of this molecule since it requires renewed molecular

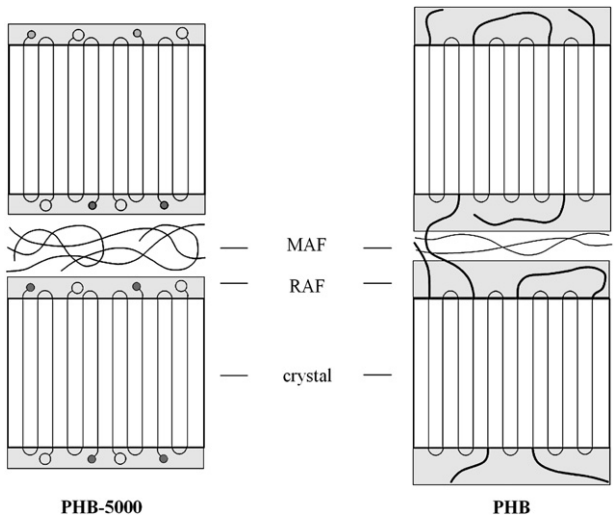

Fig. 7. Sketch of the structure of lamellae and its link to the amorphous phase in PHB-5000 (left) and PHB (right). The thickness of the crystalline layer, and of the rigid and mobile amorphous layers, approximate the phase composition of preparations of 60% crystallinity.

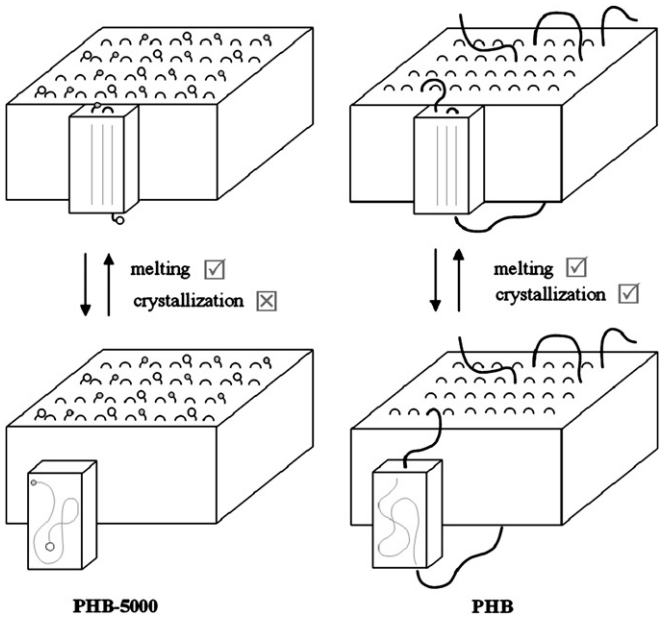

Fig. 8. Sketch of the surface structure of lamellae in PHB-5000 (left) and PHB (right), and its effect on reversible melting and crystallization. Details are explained in the text.

nucleation. In PHB of high molar mass, in contrast, melting of such a patch is not connected with a loss of the molecular nucleus due to remaining entropy-reducing covalent linkage. Therefore, nucleation-free crystallization can be observed on cooling.

Similar results regarding the effects of the length of molecules, crystal morphology, and linkage/coupling to separate phases on reversible crystallization and melting were obtained on polyethylene [26], polytetrafluoroethylene [27], or poly(oxyethylene) [48]. From this point-of-view we consider the analysis of reversible melting and crystallization of PHB of different chain length in the present work as a further evidence for validity of the concept of molecular nucleation during polymer crystallization. A major advance in excess to previous research is the consistent description of characteristic differences of the structure of the surface of crystals in PHB of different chain length, using independent concepts of characterization. The analysis of the mobility of the amorphous phase, and the analysis of reversible crystallization and melting both allow to draw qualitatively similar conclusions about the coupling of crystals and amorphous phase in semi-crystalline polymers.

References

[1] Wunderlich B. Crystal structure, morphology, defects. In: Macromolecular physics, vol. 1. New York: Academic Press; 1973.
[2] Hoffmann JD, Davis GT, Lauritzen JI. The rate of crystallization of linear polymers with chain folding. In: Hannay HB, editor. Treatise on solid state chemistry, crystalline and noncrystalline solids, vol. 3. New York: Plenum Press; 1976.
[3] Zachmann HG, Koll ZZ. Polymer 1967;216–217:180–91;
Zachmann HG, Koll ZZ. Polymer 1969;231:504–34.
[4] Wunderlich B. Crystal melting. In: Macromolecular physics, vol. 3. New York: Academic Press; 1980.
[5] Kanig G. Colloid Polym Sci 1982;260:356–77.
[6] Suzuki H, Grebowicz J, Wunderlich B. Br Polym J 1985;17:1–3;
Menczel J, Wunderlich B. J Polym Sci Part C Polym Lett 1981;19:261–4.
[7] Schick C, Krämer L, Mischok W. Acta Polym 1985;36:47–53;
Schick C, Fabry F, Schnell U, Stoll G, Deutschbein L, Mischok W. Acta Polym 1988;39:705–10;
Schick C, Wigger J, Mischok W. Acta Polym 1990;41:137–42.
[8] Androsch R, Wunderlich B. Scanning calorimetry. In: Matyjaszewski K, Gnanou Y, Leibler L, editors. Structure–property correlation and characterization techniques. Macromolecular engineering: precise synthesis, materials properties, applications, vol. 3. Weinheim: Wiley-VCH; 2007.
[9] Dlubek G, Sen Gupta A, Pionteck J, Häßler R, Krause-Rehberg R, Kaspar H, et al. Polymer 2005;46:6075–89.
[10] Rastogi R, Vellinga WP, Rastogi S, Schick C, Meijer HEH. J Polym Sci Part B Polym Phys 2004;42:2092–106.
[11] Groeninckx G, Berghmans H, Smets G. J Polym Sci Part B Polym Phys 1976;14:591–602.
[12] Wissler GE, Crist Jr B. J Polym Sci Part B Polym Phys 1980;18:1257–70.
[13] Wunderlich B. Prog Polym Sci 2003;28:383–450.
[14] Lin J, Shenogin S, Nazarenko S. Polymer 2002;43:4733–43.
[15] Olson BG, Lin J, Nazarenko S, Jamieson AM. Macromolecules 2003;36:7618–23.
[16] Androsch R, Wunderlich B. Polymer 2005;46:12556–66.
[17] Wunderlich B. J Polym Sci Part B Polym Phys 2004;42:1275–88.
[18] Wunderlich B. J Macromol Sci 2003;B42:579–98.
[19] Fischer EW, Koll ZZ. Polymer 1969;31:458–503.
[20] Strobl G, Schneider M, Voigt-Martin I. J Polym Sci Part B Polym Phys 1980;18:1361–81.
[21] Hu W, Albrecht T, Strobl G. Macromolecules 1999;32:7548–54.
[22] Okazaki I, Wunderlich B. Macromolecules 1997;30:1758–64.
[23] Ishikiriyama K, Wunderlich B. Macromolecules 1997;30:4126–31.
[24] Androsch R, Wunderlich B. Macromolecules 2001;34:5950–60.
[25] Androsch R, Wunderlich B. J Polym Sci Part B Polym Phys 2003;41:2039–51;
Androsch R, Wunderlich B. J Polym Sci Part B Polym Phys 2003;41:2157–73.
[26] Pak J, Wunderlich B. Macromolecules 2001;34:4492–503;
Pak J, Wunderlich B. J Polym Sci Part B Polym Phys 2002;40:2219–27.
[27] Androsch R. J Therm Anal Calorim 2005;79:615–22.
[28] Androsch R, Wunderlich B. Macromolecules 2000;33:9076–89.
[29] Schick C, Wurm A, Mohamed A. Thermochim Acta 2002;392–393:303–13.
[30] Schick C, Wurm A, Mohamed A. Colloid Polym Sci 2001;297:800–6.
[31] El-Taweel SH, Höhne GWH, Mansour AA, Stoll B, Seliger H. Polymer 2004;45:983–92.
[32] Saad GR, Mansour AA, Hamed AH. Polymer 1997;38:4091–6.
[33] Nogales A, Ezquerra TA, Garcia JM, Balta-Calleja FJ. J Polym Sci Part B Polym Phys 1999;37:37–49.
[34] Bergmann A, Owen A. Polym Int 2004;53:863–8.
[35] Barham PJ, Keller A, Otun EL, Holmes PA. J Mater Sci 1984;19:2781–94.
[36] Li J, Organ SJ, Hobbs JK, Terry AE, Barham PJ, Seebach D. Polymer 2004;45:8913–23.
[37] Androsch R, Radusch HJ, Funari SS. Eur Polym J 2007;43:4961–74.
[38] Wunderlich B. Thermal analysis of polymeric materials. Berlin: Springer; 2005.
[39] Mathot VBF. Calorimetry and thermal analysis of polymers. Munich: Hanser Publishers; 1994.
[40] Pyda M. NATAS Notes 2004;36:18–23.
[41] Mathot VBF, Pijpers MFJ. Thermochim Acta 1989;151:241–59.
[42] Boller A, Jin Y, Wunderlich B. J Therm Anal 1994;42:307–29.
[43] Androsch R, Moon I, Kreitmeier S, Wunderlich B. Thermochim Acta 2000;357–358:267–78.
[44] Gazzano M, Focarete ML, Riekel C, Scandola M. Biomacromolecules 2000;1:604–8.
[45] Sykes KE, McMaster TJ, Miles MJ, Barker PA, Barham PJ, Seebach D, et al. J Mater Sci 1995;30:623–7.
[46] Androsch R. Eur Polym J 2007;43:93–109.
[47] Yokouchi M, Chatani Y, Tadokoro H, Teranishi K, Tani H. Polymer 1973;14:267–72.
[48] Qiu W, Pyda M, Nowak-Pyda E, Habenschuss A, Wunderlich B. Macromolecules 2005;38:8454–67.